

Torque observation of WRSM with model uncertainties for EV applications

Yahao Chen, Malek Ghanes *Member, IEEE*, Arezki Fekik and Abdelmalek Maloum

Abstract—In this paper, we propose a torque observation method based on a linear parameter varying (LPV) approach for a wound rotor synchronous machine (WRSM) used in Electric Vehicles (EVs), specifically for the Renault ZOE. The novelty of our approach lies in its ability to handle a wide range of uncertainties and parameter variations, such as speed fluctuations and model uncertainties in both magnetic flux and resistance. This enables more accurate and robust torque estimation, which is crucial for the demanding performance requirements of EV applications. We present a comprehensive observation methodology, which includes a state and unknown input observability study, robust LPV observer design, and a convergence analysis. The effectiveness of this approach is demonstrated through both simulations and experimental tests conducted on the BEMEVE real-power test bench. To highlight its merits, the performance of the LPV observer is compared to different types of observers.

Index Terms—Wound rotor synchronous machine (WRSM), observability and observation, LPV observer, torque and flux estimation, uncertainties estimation, EV applications

I. INTRODUCTION

FOR safety and control reasons, the propulsion of electric vehicles (EVs/HEVs) is halted if the difference between the measured torque and the reference (accelerator pedal) exceeds a minimum threshold set by the manufacturers, see also [1] for various reasons of the torque ripple problems in permanent magnet synchronous machines (PMSMs). Traditional torque measurement using mechanical sensors is costly and bulky. Therefore, torque information is often obtained through data prediction systems, which can limit accuracy. To improve torque estimation accuracy and reduce costs, software-based sensor methods that do not require mechanical sensors for PMSMs have been developed in e.g., [2], [3], [4]. A sensorless torque estimation method for brushless DC motors using back electromotive force (BEMF) and observer techniques to achieve accurate torque estimation is proposed in [5]. Similarly, another approach presents a sensorless torque estimation method for induction motors using a Luenberger observer [6]. This method is based on a mathematical model of the induction motor and allows for robust torque estimation despite varying operating conditions. The methods proposed in [2], [3], [4] take into account magnetic saturation and magnet demagnetization to ensure better torque estimation accuracy. However, when validated on the full-power test bench

Yahao Chen is with HYCOMES Team, Inria Center at Rennes University, France (e-mail: yahao.chen@inria.fr).

Malek Ghanes and Arezki Fekik are with Nantes University, Centrale Nantes, LS2N UMR CNRS 6004, France (e-mail: malek.ghanes@ls2n.fr, arezki.fekik@ls2n.fr).

Abdelmalek Maloum is with Ampere, Renault, TCR, Guyancourt, France (e-mail: abdelmalek.maloum@ampere.cars).

BEMEVE (<https://renault-chair.ec-nantes.fr/bemeve>), using a wound rotor synchronous motor (WRSM) similar to those employed in early generations of the ZOE EV, the method results in real-time overruns due to the computational complexity of solving a time-varying Riccati equation. Furthermore, in [7], it is assumed that the magnetic uncertainties in the WRSM are slow-varying parameters—an assumption not adopted in the present paper—and no formal proof of this assumption is provided in [7]. Additionally, variations in stator resistance and rotor speed were not considered. A detailed comparison between the method proposed in this paper and those in [3], [7] is presented in Section IV-C. In this paper, we propose a new torque observer that takes into account to handle variations in magnetic uncertainties, stator resistances, and motor speed, thereby improving the accuracy and robustness of torque estimation. This approach is supported by experimental tests on a real-power test bench BEMEVE.

In the field of control and observation of electrical machines, model uncertainties have been a significant area of focus for researchers over the past few decades. A comprehensive survey [8] is dedicated to disturbance/uncertainty estimation and attenuation techniques for PMSMs. The electrical model uncertainties in PMSMs or AC machines primarily arise from two factors: resistance variation due to thermal effects [9] and changes in flux caused by saturation effects [10]. To address these uncertainties and disturbances, various observer-based approaches have been developed, as detailed in the survey paper [11] and the references therein. In general, for nonlinear systems, disturbance observers are employed to estimate disturbances generated by known linear exogenous systems [12] or high-order disturbances that are polynomials of time [13]. The extended state observer used in Active Disturbance Rejection Control (ADRC) [14] extends disturbances $d(t)$ by defining $\dot{d}(t) = h(t)$ and treating $d(t)$ as a state variable. This allows for the design of a differentiator-like observer with discontinuous gains to estimate $d(t)$. Additionally, extended high-gain observers [15] also use extended states to estimate the influence of uncertainties, with a constant observer gain. Also in [16], a robust integrated estimation approach estimate the states, parameters, and disturbances simultaneously for LTV systems.

To address the variations and uncertainties in the model of our WRSM, we propose a robust linear parameter varying (LPV) state observer, which differs from the aforementioned approaches in two key aspects. First, rather than treating the machine model as a nonlinear system, we leverage the LPV technique to represent the model as convex combinations of linear models and design observer gains as combinations of constant gains. This approach effectively handles speed

variations, which are treated as an external parameter entering the system in a nonlinear manner. Over the past decades, the control and observation of LPV systems have been extensively studied both theoretically and in practical applications, as highlighted in the survey by Hoffmann and Werner [17]. Notably, several works have demonstrated the effectiveness of LPV formulations for EV applications [18], [19], [20], [21], particularly for electrical machines [22], [23]. Other significant contributions to LPV-based observers can be found in [24], which uses LPV representations for globally Lipschitz nonlinear systems, and in [25], which focuses on interval observer design for LPV systems with both measured and unmeasured uncertainties, and in [26] a robust PI observer is designed and applied to a vehicle suspension platform. Second, we treat the high-order derivatives of the magnetic uncertainties as a system disturbance, $d(t)$. Instead of observing it or modeling it as a constant or slow-varying variable, we employ a robust control approach [27], [28] to suppress its impact on the estimation errors. Robust control and observation, as well-established theories, have also been widely applied in the context of electric machines [19], [22], [26], [29].

The key contributions and innovations of this paper are as follows:

- A comprehensive treatment of uncertainties and parameter variations is presented for the WRSM model. Specifically, unlike existing LPV models of electrical machines, the speed variation ω_e is treated as an LPV parameter. The magnetic uncertainties g_d , g_q , and g_f are modeled as states to be observed. Additionally, the higher-order derivatives of these magnetic uncertainties, $\ddot{g}_d = d_d$, $\ddot{g}_q = d_q$, and $\ddot{g}_f = d_f$, are considered as disturbances. Resistance uncertainties ΔR_s and ΔR_f are also included in the model, and their effects on the convergence of estimation errors are thoroughly analyzed.
- A systematic state and input observability analysis is performed for the system model, providing a clear understanding of its dynamics.
- The design of our LPV observer distinguishes itself from existing methods by incorporating both Kalman-like features [30] and enhanced robustness against disturbances. Observer gain scheduling is achieved via a finite set of linear and bilinear (quadratic) matrix inequalities (LMIs/BMIs), utilizing polytopic synthesis [31]. A novel algorithm is proposed to convert these BMIs into LMIs, which can then be efficiently solved using the Matlab LMI Toolbox.
- The proposed observer is validated through both simulation and real-time experiments conducted in different scenarios on a built-in test bench, which was developed for the EV machines of the Renault ZOE vehicle.
- The performance of the proposed observer is compared to different types of observers to further demonstrate its interest.

The remainder of the article is structured as follows: Section II presents the mathematical model of the WRSM. Section III describes the state and unknown input observability. Section IV details the robust LPV state observer design.

Section V provides the simulation results. The experimental results and discussion, demonstrating the accuracy and robustness of the proposed method, are presented in Section VI. Finally, Section VII concludes the article and outlines future research perspectives.

II. MATHEMATICAL MODEL OF WRSM

The dynamics for the flux of a WRSM in the rotor reference frame ($d - q$ frame) are given by

$$\begin{cases} \frac{d\lambda_d}{dt} = v_d - (R_s + \Delta R_s)i_d + \omega_e \lambda_q \\ \frac{d\lambda_q}{dt} = v_q - (R_s + \Delta R_s)i_q - \omega_e \lambda_d \\ \frac{d\lambda_f}{dt} = v_f - (R_f + \Delta R_f)i_f, \end{cases} \quad (1)$$

where the lower indices d , q and f indicate the d , q -frame and the excitation-frame, respectively; λ_d , λ_q , λ_f , v_d , v_q , v_f and i_d , i_q , i_f , are the flux, the voltages and currents, respectively; R_s and R_f are the resistances of the stator and of the excitation circuit, and ΔR_s and ΔR_f are differences from the measured resistances and the real ones, which are assumed to be some unknown but bounded variables; ω_e is the stator electrical angular velocity, which is assumed to be known from measurement or estimation. By considering the model uncertainties caused by e.g., nonlinear magnetic saturation, imprecise system identifications, the relation of the rotor and stator flux with the current can be represented by

$$\begin{cases} \lambda_d = L_d i_d + M_f i_f + \underbrace{\Delta L_d i_d + \Delta M_f i_f}_{g_d} \\ \lambda_q = L_q i_q + \underbrace{\Delta L_q i_q}_{g_q} \\ \lambda_f = M_f i_d + L_f i_f + \underbrace{\Delta M_f i_d + \Delta L_f i_f}_{g_f}, \end{cases}$$

where L_d , L_q , L_f are inductance of the machine, M_f denotes the d -axis-field mutual inductance. ΔL_d , ΔL_q , ΔL_f , ΔM_f are magnet model uncertainties of inductance and they are *not* assumed to be constants. All those uncertainties form compactly as g_d , g_q and g_f representing, respectively, the deviations between real and assumed flux in d , q and f -axis. The electromagnetic torque of the machine has a direct relation with the flux in $d - q$ frame:

$$T_e = \frac{3}{2}(p)(\lambda_d i_q - \lambda_q i_d), \quad (2)$$

where p is the number of pole pair of the machine. Thus to obtain the real value of the flux λ_d and λ_q in order to estimate the torque T_e , it is essential to estimate the values of the unknown variables g_d and g_q (note that the value of g_f is not necessarily needed for the torque estimation).

The flux-current relation can be rewritten in a more compact matrix form:

$$\begin{bmatrix} \lambda_d \\ \lambda_q \\ \lambda_f \end{bmatrix} = H \begin{bmatrix} i_d \\ i_q \\ i_f \end{bmatrix} + \begin{bmatrix} g_d \\ g_q \\ g_f \end{bmatrix}, \quad H = \begin{bmatrix} L_d & 0 & M_f \\ 0 & L_q & 0 \\ M_f & 0 & L_f \end{bmatrix}. \quad (3)$$

By substituting (3) into (1), we get a current model of the WRSMS as follows

$$\begin{aligned} H \cdot \frac{d}{dt} \begin{bmatrix} i_d \\ i_q \\ i_f \end{bmatrix} + \begin{bmatrix} \dot{g}_d \\ \dot{g}_q \\ \dot{g}_f \end{bmatrix} \\ = \begin{bmatrix} v_d - (R_s + \Delta R_s)i_d + \omega_e(L_q i_q + g_q) \\ v_q - (R_s + \Delta R_s)i_q - \omega_e(L_d i_d + M_f i_f + g_d) \\ v_f - (R_f + \Delta R_f)i_f \end{bmatrix}, \end{aligned} \quad (4)$$

where $\dot{g}_d, \dot{g}_q, \dot{g}_f$ are time derivatives of g_d, g_q, g_f , respectively. It is assumed in [2] or in its following works [4], [7] that those magnetic uncertainties g_d and g_q are static (i.e., $\dot{g}_d = \dot{g}_q = 0$) or slowing-varying variables (i.e., $\dot{g}_d = \dot{g}_q = 0$). In the present paper, we do not make such assumptions. Instead we regard the higher order time derivatives of the magnetic uncertainties as external disturbances injected to the system, namely, we denote

$$\begin{bmatrix} \dot{g}_d \\ \dot{g}_q \\ \dot{g}_f \end{bmatrix} = \begin{bmatrix} c_d \\ c_q \\ c_f \end{bmatrix}, \quad \begin{bmatrix} \dot{c}_d \\ \dot{c}_q \\ \dot{c}_f \end{bmatrix} = \begin{bmatrix} d_d \\ d_q \\ d_f \end{bmatrix}. \quad (5)$$

The angular velocity ω_e can be obtained or estimated in real time by angular position/rate sensors or using high-frequency injection methods [32]–[34]. Then based on different views of the time-varying variable $\omega_e = \omega_e(t)$, the mathematical model of the machine can be formulated into either a linear parameter varying (LPV) system or a nonlinear system. It can be observed from (4) that the right-hand-side of the equation depends affinely on the current variables i_d, i_q, i_f and the only nonlinearities come from the bi-linearity of ω_e and the current variables. By treating ω_e as a varying parameter instead of a time-varying variable, the combination of (4) and (5) gives an LPV system in the form

$$\Sigma(\omega_e) : \begin{cases} \dot{x} = A(\omega_e)x + Bu + \Delta Ax + Ed \\ y = Cx, \end{cases} \quad (6)$$

where $x = (i_d, i_q, i_f, g_d, g_q, c_d, c_q, c_f) \in \mathbb{R}^8$ are states, $u = (v_d, v_q, v_f) \in \mathbb{R}^3$ are known inputs and $d = (d_d, d_q, d_f) \in \mathbb{R}^3$ are unknown disturbances. Denote $L_\delta := M_f^2 - L_d L_f$, the system matrices are given by, respectively,

$$\begin{aligned} A(\omega_e) &= \\ &\left[\begin{array}{ccccccc} \frac{R_s L_f}{L_\delta} & \frac{-L_f L_q \omega_e}{L_\delta} & \frac{-R_f M_f}{L_\delta} & 0 & \frac{-L_f \omega_e}{L_\delta} & \frac{L_f}{L_\delta} & 0 & \frac{-M_f}{L_\delta} \\ \frac{-\omega_e L_d}{L_q} & \frac{-R_s}{L_q} & \frac{-\omega_e M_f}{L_q} & \frac{-\omega_e}{L_q} & 0 & 0 & \frac{-1}{L_q} & 0 \\ \frac{-R_s M_f}{L_\delta} & \frac{M_f L_q \omega_e}{L_\delta} & \frac{R_f L_d}{L_\delta} & 0 & \frac{M_f \omega_e}{L_\delta} & \frac{-M_f}{L_\delta} & 0 & \frac{L_d}{L_\delta} \\ 0 & 0 & 0 & 0 & 0 & 1 & 0 & 0 \\ 0 & 0 & 0 & 0 & 0 & 0 & 1 & 0 \\ 0 & 0 & 0 & 0 & 0 & 0 & 0 & 0 \\ 0 & 0 & 0 & 0 & 0 & 0 & 0 & 0 \\ 0 & 0 & 0 & 0 & 0 & 0 & 0 & 0 \end{array} \right], \\ B &= \left[\begin{array}{ccccccc} \frac{-L_f}{L_\delta} & 0 & \frac{M_f}{L_\delta} & 0 & 0 & 0 & 0 \\ 0 & \frac{1}{L_q} & 0 & 0 & 0 & 0 & 0 \\ \frac{M_f}{L_\delta} & 0 & \frac{-L_d}{L_\delta} & 0 & 0 & 0 & 0 \end{array} \right]^T, \quad C = \left[\begin{array}{ccccccc} 1 & 0 & 0 & 0 & 0 & 0 & 0 \\ 0 & 1 & 0 & 0 & 0 & 0 & 0 \\ 0 & 0 & 1 & 0 & 0 & 0 & 0 \end{array} \right], \\ E &= \left[\begin{array}{ccc} 0 & 0 & 0 \\ 0 & 0 & 0 \\ 0 & 0 & 0 \\ 0 & 0 & 0 \\ 1 & 0 & 0 \\ 0 & 1 & 0 \\ 0 & 0 & 1 \end{array} \right], \quad \Delta A = \left[\begin{array}{ccccccc} \frac{\Delta R_s L_f}{L_\delta} & 0 & \frac{-\Delta R_f M_f}{L_\delta} & 0 & 0 & 0 & 0 \\ 0 & \frac{-\Delta R_s}{L_q} & 0 & 0 & 0 & 0 & 0 \\ \frac{-\Delta R_s M_f}{L_\delta} & 0 & \frac{\Delta R_f L_d}{L_\delta} & 0 & 0 & 0 & 0 \\ 0 & 0 & 0 & 0 & 0 & 0 & 0 \\ 0 & 0 & 0 & 0 & 0 & 0 & 0 \\ 0 & 0 & 0 & 0 & 0 & 0 & 0 \\ 0 & 0 & 0 & 0 & 0 & 0 & 0 \end{array} \right]. \end{aligned}$$

Remark 1. Generally, the model uncertainties arising from variations in resistance, ΔR_s and ΔR_f , can be viewed as slow-varying parameters in the system matrix or as external disturbances. However, here we do not regard them as varying parameters like ω_e . This exclusion stems from the challenge of accurately determining the bounds of these variations, which are necessary for robust LPV observer design. While both ΔR_s and ΔR_f are bounded, determining their values or bounds precisely is difficult. There are two reasons why these uncertainties are not treated as external disturbances d . Firstly, an examination of ΔA and B reveals that the resistance uncertainties and the known inputs u affect the system in similar directions. In cases where input voltages are sufficiently large, they can compensate for any adverse effects caused by ΔR_s and ΔR_f . Secondly, the primary objective of the LPV observer design below is to bolster robust performance against magnetic uncertainties rather than resistance uncertainties.

In practical systems, the angular velocity of the machine operates within a limited range due to physical constraints. Therefore, it is reasonable to assume that the parameter ω_e is bounded, meaning it falls within a specified range, i.e.,

$$\omega_e \in [\underline{\omega}_e, \bar{\omega}_e],$$

where $\bar{\omega}_e = \max(\omega_e)$ and $\underline{\omega}_e = \min(\omega_e)$ are constants. System (6) is called a *polytopic* LPV system [17], [35] because the system matrix A dependents affinely on the varying parameter ω_e , i.e.,

$$A(\omega_e) \in \text{Co}\{A(\underline{\omega}_e), A(\bar{\omega}_e)\},$$

where $\text{Co}\{\cdot\}$ denotes a convex hull of matrices. More specifically, we can write

$$A(\omega_e) = \alpha(\omega_e)A(\underline{\omega}_e) + (1 - \alpha(\omega_e))A(\bar{\omega}_e),$$

where

$$0 \leq \alpha(\omega_e) = \frac{\bar{\omega}_e - \omega_e}{\bar{\omega}_e - \underline{\omega}_e} \leq 1. \quad (7)$$

Remark 2. Although this is not the case for our test bench (see the experimental results in Section VI), some systems may exhibit a very large speed range $[\underline{\omega}_e, \bar{\omega}_e]$. To handle widely varying parameters, the interval can be divided into sub-ranges $[\omega_0, \omega_1], [\omega_1, \omega_2], \dots, [\omega_{m-1}, \omega_m]$, where $\omega_0 = \underline{\omega}_e$ and $\omega_m = \bar{\omega}_e$. Then, we express $A(\omega_e)$ as

$$A(\omega_e) = \sum_{i=0}^m \alpha_i(\omega_e),$$

where $0 \leq \alpha_i(\omega_e) \leq 1$ and $\sum_{i=0}^m \alpha_i(\omega_e) = 1$. The observer design follows a similar approach as in Section V. However, as the number m of sub-ranges increases, the computational cost also rises: the explicit expressions for each $\alpha_i(\omega_e)$ become more complex, and the number of LMIs/BMIs (see Corollary 1) to be solved increases accordingly.

Apart from the angular velocity, due to the physical operation limits and the reasons that the currents of the machine has already been regulated via a PI controller, we make the following boundness assumptions on the variables x , the

resistance uncertainties $\Delta R_s, \Delta R_f$ (or, equivalently, ΔA) and the acceleration $\dot{\omega}_e$.

Assumption 1. There exist positive scalars l_1, l_2, τ such that

$$\|\Delta A\| < l_1, \quad \|x\| < l_2, \quad \|\dot{\omega}_e\| < \tau.$$

If the angular velocity ω_e is viewed as a known input variable, then system (6) can be seen as a nonlinear system

$$\Sigma : \begin{cases} \dot{x} = f(x, \omega_e, \Delta R_s, \Delta R_f) + Bu + Ed \\ y = h(x), \end{cases} \quad (8)$$

where $f(x, \omega_e, \Delta R_s, \Delta R_f) = (A(\omega_e) + \Delta A)x, h(x) = Cx$. This nonlinear system model will be used for checking the state and unknown inputs/disturbance observability. Then a robust LPV observer will be built on system (6).

III. STATE AND UNKNOWN INPUT OBSERVABILITY

We adopt the classical definition of state observability for nonlinear systems in e.g., [36], [37]. Denote a solution of Σ starting from an initial point x^0 under some ω_e, u, d by $x(t, x^0; \omega_e, u, d)$.

Definition 1 (State observability). The system Σ is called locally state observable if there exists an open dense subset $V \subseteq \mathbb{R}^n$ and a time scalar $T > 0$ such that for any two states $x^1 \in V$ and $x^2 \in V$, the corresponding outputs with x^1 and x^2 as initial points satisfies that $y(t, x^1; \omega_e, u, d) \neq y(t, x^2; \omega_e, u, d)$ implies $x(t, x^1; \omega_e, u, d) \neq x(t, x^2; \omega_e, u, d)$ for all $t \in [0, T]$ and for all admissible u, d, ω_e .

Roughly speaking, the state observability is a property for the reconstruction of the state variables x via the data from the measurable outputs y and its time derivatives \dot{y}, \ddot{y}, \dots when assuming the inputs ω_e, u and d (and their time derivatives) are known. However, the disturbance d , a priori, is not given, to know if it is possible to use the available information y to recover d , we need to check its unknown input observability, the latter concept is closely related to the left-invertibility of nonlinear control systems [37]–[39].

Definition 2 (Left-invertibility and unknown input observability). The system Σ is called locally left-invertible with respect to inputs d and outputs y if there exists an open dense subset $V \subseteq \mathbb{R}^n$ and a time scalar $T > 0$ such that for any initial point $x^0 \in V$ and two admissible inputs $d^1(t)$ and $d^2(t)$, the corresponding outputs with d^1 and d^2 as inputs satisfies that $y(t, x^0; \omega_e, u, d^1) \neq y(t, x^0; \omega_e, u, d^2)$ implies $d^1(t) \neq d^2(t)$ for all $t \in [0, T]$ and for all admissible u, ω_e . The system Σ is called locally unknown input observable for d if it is locally left-invertible without knowing the initial value x^0 .

The input-observability characterizes the property of recovering the unknown inputs d by $y, \dot{y}, \ddot{y}, \dots$ (possible need the help of u, ω_e and their derivatives) without the knowledge of x^0 . The criteria for checking the state or unknown input observability relies on the calculation of the time derivative array for the outputs y .

Remark 3. Recall the definition of *vector relative degree* [37], [40]: For a system Σ with $\dim y = \dim d = m$, the system

has a (vector) relative degree $r = (r_1, \dots, r_m)$ at a point x^0 with respect to the outputs y and inputs d if the following conditions hold: 1. For all $1 \leq i, j \leq m$ and $k < r_i - 1$, we have $\frac{\partial y_i^{(k)}}{\partial d_j}(x, \Omega_e^{(k)}, U^{(k)}) \equiv 0$, where $\Omega_e^{(k)} = (\omega_e, \dots, \omega_e^{(k)})$ and $U^{(k)} = (u, \dots, u^{(k)})$. 2. The $m \times m$ decoupling matrix $D(x^0, \Omega_e^{(R)}, U^{(R)}) = \frac{\partial y_i^{(r_i)}}{\partial d_j}(x^0, \Omega_e^{(R)}, U^{(R)})$, for $1 \leq i, j \leq m$, where $R = \max(r_i)$, is invertible. Thus, if the (vector) relative degree r is well-defined for Σ , we have the relationship:

$$y^{(r)} = F(x, \Omega_e^{(R)}, U^{(R)}) + D(x, \Omega_e^{(R)}, U^{(R)})d,$$

for some vector-valued function F . It follows that the input d can be expressed as

$$d = D^{-1}(y^{(r)} - F(x, \Omega_e^{(R)}, U^{(R)})),$$

around $x = x^0$. Therefore, the map from d to y is injective for fixed x^0, ω_e , and u , meaning that Σ is left-invertible with respect to y and d , as per Definition 2.

Denote $L_f h(x, \omega_e) := \frac{\partial h(x, \omega_e)}{\partial x} f(x, \omega_e)$. For system Σ , given by (8), we have

$$\dot{y} = L_f h(x, \omega_e) + L_B h \cdot u + L_E h \cdot d,$$

where

$$L_f h(x, \omega_e) = C(A(\omega_e) + \Delta A)x, \quad L_B h = CB, \quad L_E h = 0.$$

Then

$$\begin{aligned} \dot{y} &= L_f^2 h(x, \omega_e) + \frac{\partial L_f h}{\partial \omega_e}(x) \dot{\omega}_e + L_B L_f h(\omega_e) \cdot u \\ &\quad + L_E L_f h \cdot d + L_B h \cdot \dot{u} + L_E h \cdot \dot{d}, \end{aligned}$$

where

$$L_f^2 h(x, \omega_e) = C(A(\omega_e) + \Delta A)^2 x, \quad \frac{\partial L_f h}{\partial \omega_e}(x) = C \frac{\partial A(\omega_e)}{\partial \omega_e} x,$$

$$L_B L_f h(\omega_e) = C(A(\omega_e) + \Delta A)B,$$

$$L_E L_f h = C(A(\omega_e) + \Delta A)E.$$

It can be seen that the Jacobian matrix

$$O(\omega_e, \dot{\omega}_e) = \frac{\partial(y, \dot{y}, \ddot{y})}{\partial x} = \begin{bmatrix} C & & & & & & & \\ C(A(\omega_e) + \Delta A) & & & & & & & \\ C(A(\omega_e) + \Delta A)^2 + C \frac{\partial A(\omega_e)}{\partial \omega_e} \dot{\omega}_e & & & & & & & \\ \hline 1 & 0 & 0 & 0 & 0 & 0 & 0 & 0 \\ 0 & 1 & 0 & 0 & 0 & 0 & 0 & 0 \\ 0 & 0 & 1 & 0 & 0 & 0 & 0 & 0 \\ \frac{\tilde{R}_s L_f}{L_\delta} & \frac{-L_f L_q \omega_e}{L_\delta} & \frac{-\tilde{R}_f M_f}{L_\delta} & 0 & \frac{-L_f \omega_e}{L_\delta} & \frac{L_f}{L_\delta} & 0 & \frac{-M_f}{L_\delta} \\ \frac{-\omega_e L_d}{L_q} & \frac{-\tilde{R}_s}{L_q} & \frac{-\omega_e M_f}{L_q} & \frac{-\omega_e}{L_q} & 0 & 0 & 0 & \frac{-1}{L_q} \\ \frac{-\tilde{R}_s M_f}{L_\delta} & \frac{M_f L_q \omega_e}{L_\delta} & \frac{\tilde{R}_f L_d}{L_\delta} & 0 & \frac{M_f \omega_e}{L_\delta} & \frac{-M_f}{L_\delta} & 0 & \frac{L_d}{L_\delta} \\ * & * & * & A_{74} & A_{75} & A_{76} & A_{77} & A_{78} \\ * & * & * & A_{84} & A_{85} & A_{86} & A_{87} & A_{88} \\ * & * & * & A_{94} & A_{95} & A_{96} & A_{97} & A_{98} \end{bmatrix},$$

where $\tilde{R}_s = R_s + \Delta R_s, \tilde{R}_f = R_f + \Delta R_f, A_{74} = \frac{L_f}{L_\delta} \omega_e^2, A_{75} = -\frac{L_f^2 \tilde{R}_s}{L_\delta^2} \omega_e - \frac{\tilde{R}_f M_f^2}{L_\delta^2} \omega_e - \frac{L_f}{L_\delta} \dot{\omega}_e, A_{76} = \frac{\tilde{R}_s L_f^2}{L_\delta^2} + \frac{\tilde{R}_f M_f^2}{L_\delta^2} - \frac{L_f}{L_\delta} \omega_e, A_{77} = 0, A_{78} = -\frac{\tilde{R}_s L_f M_f}{L_\delta^2} - \frac{\tilde{R}_f M_f L_d}{L_\delta^2}, A_{84} = \frac{\tilde{R}_s}{L_q^2} \omega_e - \frac{1}{L_q} \dot{\omega}_e, A_{85} = -\frac{1}{L_q} \omega_e^2, A_{86} = 0, A_{87} = \frac{\tilde{R}_s}{L_q^2}, A_{88} = 0, A_{94} = -\frac{M_f}{L_\delta} \omega_e^2, A_{95} = \frac{\tilde{R}_s M_f L_f}{L_\delta^2} \omega_e + \frac{\tilde{R}_f M_f L_d}{L_\delta^2} \omega_e + \frac{M_f}{L_\delta} \dot{\omega}_e, A_{96} = -\frac{\tilde{R}_s M_f L_f}{L_\delta^2} - \frac{\tilde{R}_f L_d M_f}{L_\delta^2} + \frac{M_f}{L_\delta} \omega_e, A_{97} = 0, A_{98} = \frac{\tilde{R}_s M_f^2}{L_\delta^2} + \frac{\tilde{R}_f L_f^2}{L_\delta^2}$

and the symbol “*” represents irrelevant terms. The following results concern with the state and unknown input observability of the system.

Theorem 1. *The system Σ , given by (8), is state observable for all $x \in \mathbb{R}^n$ if and only if*

$$|\dot{\omega}_e| \neq \omega_e^2. \quad (9)$$

Moreover, Σ is left-invertible with respect to the unknown input d but it is not unknown input observable.

Proof. We can find two matrix-valued functions $P(\omega_e) \in \mathbb{R}^{9 \times 9}$ and $Q(\omega_e) \in \mathbb{R}^{8 \times 8}$, which are invertible for all $\omega_e \in \mathbb{R}$, such that $\tilde{O}(\omega_e, \dot{\omega}_e) = P(\omega_e)O(\omega_e, \dot{\omega}_e)Q(\omega_e) =$

$$\begin{bmatrix} 1 & 0 & 0 & 0 & 0 & 0 & 0 & 0 & 0 \\ 0 & 1 & 0 & 0 & 0 & 0 & 0 & 0 & 0 \\ 0 & 0 & 1 & 0 & 0 & 0 & 0 & 0 & 0 \\ 0 & 0 & 0 & 0 & \frac{L_f}{L_\delta} & 0 & -\frac{M_f}{L_\delta} \\ 0 & 0 & 0 & 0 & \frac{L_f}{L_\delta} & 0 & -\frac{M_f}{L_\delta} \\ 0 & 0 & 0 & 0 & 0 & \frac{-1}{L_q} & 0 \\ 0 & 0 & 0 & 0 & 0 & 0 & \frac{L_d}{L_\delta} \\ 0 & 0 & 0 & \omega_e^2 & \dot{\omega}_e & 0 & 0 \\ 0 & 0 & 0 & \omega_e^2 & \omega_e & 0 & 0 \\ 0 & 0 & 0 & 0 & 0 & 0 & 0 \end{bmatrix}.$$

Recall from Corollary 4.11 of [37] that the system Σ is state-observable if and only if $\text{rank } O(\omega_e, \dot{\omega}_e) = 8$. The matrix \tilde{O} (and thus O) is of rank 8 if and only if the matrix $\begin{bmatrix} \omega_e^2 & \dot{\omega}_e \\ \dot{\omega}_e & \omega_e^2 \end{bmatrix}$ is non-singular. The latter condition is equivalent to (9). Hence Σ is state observable if and only if (9) holds.

Moreover, it can be seen from the calculations of \dot{y} and \ddot{y} that the vector relative degree [37], [40] of Σ with respect to y and d is $(2, 2, 2)$ since $L_E h = 0$ and $L_E L_f h$ is invertible. So the system Σ is left-invertible with respect to y and d because $d = (L_E L_f h)^{-1}(\ddot{y} - L_f^2 h(x, \omega_e) - \frac{\partial L_f h}{\partial \omega_e}(x) \dot{\omega}_e - L_B L_f h(\omega_e) \cdot u - L_B h \cdot \dot{u})$. Thus given the same initial condition x^0 , any two different outputs $y^1(t, x^0; \omega_e, u, d^1) \neq y^2(t, x^0; \omega_e, u, d^2)$ must imply $d^1(t) \neq d^2(t)$. However, since it is not possible to express x (and thus x^0 and d) as some functions of y , \dot{y} , u , \dot{u} , ω , $\dot{\omega}$ if x^0 is unknown, we have that $y^1(t, x^0; \omega_e, u, d^1) \neq y^2(t, \tilde{x}^0; \omega_e, u, d^2)$ does not necessarily imply $d^1(t) \neq d^2(t)$. Therefore, Σ is not unknown input observable for d . \square

Remark 4. (i) The ranks of $O(\omega_e, \dot{\omega}_e)$ and $L_E L_f h$, and thus the state observability and unknown input observability of Σ , are not determined by the resistance uncertainties ΔR_s and ΔR_f . However, in order to exactly estimate $x(t)$ or $d(t)$ using x^0 , $y(t)$, $u(t)$, $\omega_e(t)$ and their derivatives, the precise values of the resistances are necessary. Although the latter data is not available, we can still design an observer to estimate the state $x(t)$ with bounded errors if ΔR_s and ΔR_f are assumed to be bounded.

(ii) Since $d(t)$ are not observable via the outputs y , we will treat them as unknown disturbances, to minimum its side effect to a state observer, the robustness of the observer against external disturbances should be addressed during design process.

IV. ROBUST LPV STATE OBSERVER

A. Observer design

Now for the polytopic LPV system $\Sigma(\omega_e)$, we seek a Kalman-like LPV observer in the form

$$\hat{\Sigma}(\omega_e) : \begin{cases} \dot{\hat{x}} = A(\omega_e)\hat{x} + Bu + K(\omega_e)(y - C\hat{x}) \\ \hat{y} = \hat{C}\hat{x} \end{cases} \quad (10)$$

where $\hat{x} = (\hat{i}_d, \hat{i}_q, \hat{i}_f, \hat{g}_d, \hat{g}_q, \hat{c}_d, \hat{c}_q, \hat{c}_f) \in \mathbb{R}^8$ are the states of the observer, $K(\omega_e) \in \mathbb{R}^{8 \times 3}$ is the observer gain which will be designed below and

$$\hat{C} = \begin{bmatrix} 0 & 0 & 0 & 1 & 0 & 0 & 0 & 0 \\ 0 & 0 & 0 & 0 & 1 & 0 & 0 & 0 \end{bmatrix},$$

which is defined for the robust performance on the estimations of g_d and g_q . Define the error e as the difference between the real states x and the estimated ones \hat{x} ,

$$e := x - \hat{x}.$$

Then the dynamics of the error and the performance outputs $y_e := \hat{C}x - \hat{y}$ are given by

$$\begin{cases} \dot{e} = (A(\omega_e) - K(\omega_e)C)e + Ed + \Delta Ax \\ y_e = \hat{C}e. \end{cases}$$

In order to minimize the effect of the disturbance for the estimation, our objective to design a robust LPV observer defined below, see also similar definitions in [20], [26].

Definition 3. The observer $\hat{\Sigma}(\omega_e)$ is called a robust LPV H_∞ observer for system $\Sigma(\omega_e)$ with performance $\gamma > 0$ if

- (i) $e(t) \rightarrow 0$ as $t \rightarrow \infty$ when $d = 0$ and $\Delta R_s = \Delta R_f = 0$.
- (ii) $\sup_{\omega_e \in [\underline{\omega}_e, \bar{\omega}_e]} \sup_{||d||_2 \neq 0} \frac{||y_e||_2}{||d||_2} \leq \gamma$.

In the above definition, the L_2 norm of u is $||u||_2^2 := \int_0^\infty u^T u dt$ and the supremum is taken over all nonzero trajectories of the error dynamics starting from $e(0) = 0$. The following theorem states sufficient conditions for the existence of a robust LPV H_∞ observers for system $\Sigma(\omega_e)$.

Theorem 2. *Under Assumption 1, there exists a robust LPV H_∞ observer $\hat{\Sigma}(\omega_e)$ for system $\Sigma(\omega_e)$ if there exist a matrix-valued function $P(\omega_e) = P^T(\omega_e) > 0$ and a positive scalar $\gamma > 0$ such that $\forall \omega_e \in [\underline{\omega}_e, \bar{\omega}_e]$:*

$$\begin{bmatrix} S(\omega_e) & P(\omega_e) & P(\omega_e)E & \hat{C}^T \\ P(\omega_e) & -Q^{-1} & 0 & 0 \\ E^T P(\omega_e) & 0 & -\gamma I & 0 \\ \hat{C} & 0 & 0 & -\gamma I \end{bmatrix} < 0, \quad (11)$$

where

$$S(\omega_e) = A(\omega_e)^T P(\omega_e) + P(\omega_e)A(\omega_e) - C^T R^{-1} C \pm \tau \frac{\partial P(\omega_e)}{\partial \omega_e},$$

and $Q = Q^T > 0$, $R = R^T > 0$ are constant weighing matrices to tune. The observer gain is given by $K(\omega_e) = P^{-1}(\omega_e)C^T R^{-1}$. Moreover, if the resistances uncertainties ΔR_s and ΔR_f are not zero but bounded, then the errors $e(t)$ are also bounded.

Proof. Consider a Lyapunov function candidate:

$$V(e, t) = e^T P(\omega_e(t))e.$$

It follows that

$$\begin{aligned} \frac{dV(e, t)}{dt} &= \dot{e}^T P(\omega_e) e + e^T \dot{P}(\omega_e) e + e^T P(\omega_e) \dot{e} \\ &= e^T (A^T(\omega_e) P(\omega_e) - C^T R^{-1} C) e + d^T E^T P(\omega_e) e + \\ &\quad x^T (\Delta A)^T e + e^T \dot{\omega}_e \frac{\partial P(\omega_e)}{\partial \omega_e} e + e^T P(\omega_e) E d + \\ &\quad e^T \Delta A x + e^T (P(\omega_e) A(\omega_e) - C^T R^{-1} C) e \\ &= e^T (A^T(\omega_e) P(\omega_e) + P(\omega_e) A(\omega_e) - C^T R^{-1} C) e + \\ &\quad \dot{\omega}_e e^T \left(\frac{\partial P(\omega_e)}{\partial \omega_e} \right) e + d^T E^T P(\omega_e) e + e^T P(\omega_e) E d + \\ &\quad x^T (\Delta A)^T e + e^T \Delta A x - e^T C^T R^{-1} C e. \end{aligned}$$

Now if (11) holds, then, by Schur complement, we have

$$\begin{bmatrix} S(\omega_e) + P(\omega_e) Q P(\omega_e) & P(\omega_e) E \\ E^T P(\omega_e) & -\gamma^2 I \end{bmatrix} + \begin{bmatrix} \hat{C}^T \\ 0 \end{bmatrix} \begin{bmatrix} \hat{C} & 0 \end{bmatrix} < 0$$

That means

$$\begin{aligned} e^T (S(\omega_e) + P(\omega_e) Q P(\omega_e)) e + d^T E^T P(\omega_e) e + d^T P(\omega_e) E e \\ + y_e^T y_e - \gamma^2 d^T d < 0. \end{aligned}$$

As a consequence, we have

$$\begin{aligned} f(\omega_e, \dot{\omega}_e) := \\ e^T (A^T(\omega_e) P(\omega_e) + P(\omega_e) A(\omega_e) - C^T R^{-1} C) e + \\ e^T \left(P(\omega_e) Q P(\omega_e) + \dot{\omega}_e \frac{\partial P(\omega_e)}{\partial \omega_e} \right) e + d^T E^T P(\omega_e) e + \\ e^T P(\omega_e) E d + y_e^T y_e - \gamma^2 d^T d < 0. \end{aligned} \tag{12}$$

It follows that

$$\begin{aligned} \frac{dV(e, t)}{dt} + y_e^T y_e - \gamma^2 d^T d + e^T P(\omega_e) Q P(\omega_e) e + \\ e^T C^T R^{-1} C e - x^T (\Delta A)^T e - e^T \Delta A x = f(\omega_e, \dot{\omega}_e) < 0. \end{aligned} \tag{13}$$

If $\Delta R_s = \Delta R_f = 0$, then $\Delta A = 0$ and thus

$$\begin{aligned} \frac{dV(e, t)}{dt} + y_e^T y_e - \gamma^2 d^T d &< -e^T P(\omega_e) Q P(\omega_e) e \\ &\quad - e^T C^T R^{-1} C e < 0. \end{aligned}$$

Conditions (i) of Definition 3 is satisfied because $\frac{dV(e, t)}{dt}$ is negative when $d = 0$. It follows by classical robust control theory [28] that condition (ii) is also satisfied. Indeed, by integration, we have that for any $T > 0$:

$$\int_0^T \left(\frac{dV(e, t)}{dt} + y_e^T y_e - \gamma^2 d^T d \right) dt < 0.$$

Taking into account $e(0) = 0$, it follows that

$$e^T(T) P(\omega_e) e(T) + \int_0^T y_e^T y_e dt < \gamma^2 \int_0^T d^T d dt.$$

By taking $T = \infty$, we can conclude that $\frac{\|y_e\|_2}{\|d\|_2} < \gamma$. Therefore, $\hat{\Sigma}(\omega_e)$ is a robust LPV observer. Moreover, consider the case that ΔR_s and ΔR_f are nonzero. Recall from Assumption 1 that $\|\Delta A\| < l_1$ and $\|x\| < l_2$. Since

$P(\omega_e) Q P(\omega_e) + C^T R^{-1} C > 0$, there exists $\lambda > 0$ such that $\|P(\omega_e) Q P(\omega_e) + C^T R^{-1} C\| > \lambda$. Then by (13), we have

$$\frac{dV(e, t)}{dt} < -\lambda \|e\|^2 + l_1 l_2 \|e\| - y_e^T y_e + \gamma^2 d^T d.$$

Hence $e(t)$ is bounded by $\frac{l_1 l_2}{\lambda}$ because for $\|e(t)\| > \frac{l_1 l_2}{\lambda}$ and d tends to zero, we have $\frac{dV(e, t)}{dt} < 0$. \square

Remark 5. The observer $\hat{\Sigma}(\omega_e)$ is referred to as a Kalman-like observer because the gain $K(\omega_e)$ is designed following principles similar to those of the original Kalman observer [30], where the gain is determined to minimize the estimation error covariance in the presence of Gaussian noise. More explicitly, the stochastic model as $\dot{x} = A(\omega_e)x + Bu + w$, $y = Cx + v$, where w and v are Gaussian noises for process and measurement, respectively. Although we do not handle a fully stochastic model with noise, the observer gain is obtained by solving Riccati inequalities in a manner reminiscent of the Kalman framework. As a result, the tuning matrices Q and R -which represent the covariance of w and v in the standard Kalman observer-are employed here as weighting matrices. These matrices enable us to adjust the relative emphasis placed on the system model and measurement output, respectively.

B. Polytopic LPV synthesis

In order use the above results to find an observer gain $K(\omega_e)$, we need to render the infinite set of LMIs in (11) to a finite set of LMIs (or BMIs). There are different approaches for LPV synthesis as shown in the survey [17] and the references therein. Since our LPV system $\Sigma(\omega_e)$ is polytopic and only the system matrix A depends on ω_e , we will use the *polytopic synthesis* [31], [35]. Denote

$$A_1 = A(\underline{\omega}_e) \text{ and } A_2 = A(\bar{\omega}_e).$$

Corollary 1. Under Assumption 1, there exists a robust LPV H_∞ observer if there exist two positive-definite constant matrices $P_1 = P_1^T > 0$, $P_2 = P_2^T > 0$ and a positive scalar $\gamma > 0$ such that $\forall i, j = 1, 2$:

$$\begin{bmatrix} A_i^T P_i + P_i A_i - C^T R^{-1} C + \tilde{\tau}(P_i - P_j) & P_i & P_i E & \hat{C}^T \\ P_i & -Q^{-1} & 0 & 0 \\ E^T P_i & 0 & -\gamma I & 0 \\ \hat{C} & 0 & 0 & -\gamma I \end{bmatrix} < 0, \tag{14a}$$

$$(A_1 - A_2)^T (P_1 - P_2) + (P_1 - P_2)(A_1 - A_2) + (P_1 - P_2)Q(P_1 - P_2) \geq 0, \tag{14b}$$

where $\tilde{\tau} = \frac{\tau}{\bar{\omega}_e - \underline{\omega}_e}$, $Q = Q^T > 0$ and $R = R^T > 0$ are tuning matrices. The observer gain $K(\omega_e) = P^{-1}(\omega_e) C^T R^{-1}$, where $P(\omega_e) = \alpha(\omega_e)P_1 + (1 - \alpha(\omega_e))P_2$ and α is given by (7).

Proof. Observe that $f(\omega_e, \dot{\omega}_e)$ of (12) is a quadratic function of ω_e . By Lemma 3.1 of [31], $\forall \omega_e \in [\underline{\omega}_e, \bar{\omega}_e]$ and $\forall |\dot{\omega}_e| < \tilde{\tau}(\bar{\omega}_e - \underline{\omega}_e)$: $f(\omega_e) < 0$ if

$$\frac{\partial^2 f(\omega_e, \dot{\omega}_e)}{\partial \omega_e^2} = \left(\frac{\partial \alpha(\omega_e)}{\partial \omega_e} \right)^2 \frac{\partial^2 f}{\partial \alpha^2} \geq 0, \tag{15}$$

together with $\forall \omega_e \in \{\underline{\omega}_e, \bar{\omega}_e\}$ and $\forall \dot{\omega}_e \in \{-\tilde{\tau}(\bar{\omega}_e - \underline{\omega}_e), \tilde{\tau}(\bar{\omega}_e - \underline{\omega}_e)\}$:

$$f(\omega_e, \dot{\omega}_e) < 0. \quad (16)$$

Observe that

$$\begin{aligned} \frac{\partial^2 f}{\partial \alpha^2} = e^T ((A_1 - A_2)^T (P_1 - P_2) + (P_1 - P_2)(A_1 - A_2) \\ + (P_1 - P_2)Q(P_1 - P_2))e, \end{aligned}$$

thus (14b) implies (15). Moreover, by using Schur complement and $\frac{\partial P(\omega_e)}{\partial \omega_e} = \frac{1}{\bar{\omega}_e - \underline{\omega}_e}(P_1 - P_2)$, it is seen that (14a) guarantees (16) holds at the corners of the ranges for ω_e and $\dot{\omega}_e$. Therefore, with the same arguments in the proof of Theorem 2, we can conclude that $K(\omega_e) = P^{-1}(\omega_e)C^T R^{-1}$ with $P(\omega_e) = \alpha P_1 + (1 - \alpha)P_2$ is the observer gain for a robust LPV observer. \square

Note that the constraint (14b) is not an LMI but a BMI which depends quadratically on the unknowns and it is a *non-convex* optimization problem if one wants to minimize γ . It is not possible to transform simultaneously both (14a) and (14b) into LMIs by Schur complement or changing of variables. To solve this problem, one may use e.g. the methods in [41], [42]. Here we propose a simple solution with possible conservatism but easy for calculation and realization.

Step 1: Minimize $\gamma > 0$ under the LMIs constraints (14a) and

$$(A_1 - A_2)^T (P_1 - P_2) + (P_1 - P_2)(A_1 - A_2) + L_0 \geq 0, \quad L_0 > 0.$$

Denote the resulting P_1 and P_2 as P_{10} and P_{20} .

Step 2: If $L_0 \leq (P_{10} - P_{20})Q(P_{10} - P_{20})$, then stop and return to P_{10} and P_{20} . Otherwise, set $k = 1$ and go to Step 3.

Step 3: Minimize $\gamma > 0$ under the LMIs constraints (14a) and

$$\begin{aligned} (A_1 - A_2)^T (P_1 - P_2) + (P_1 - P_2)(A_1 - A_2) + L_k \geq 0, \\ L_{k-1} - L_k > 0. \end{aligned}$$

Denote the resulting P_1 and P_2 as P_{1k} and P_{2k} .

Step 4: If $L_k \leq (P_{1k} - P_{2k})Q(P_{1k} - P_{2k})$, then stop and return to P_{1k} and P_{2k} . Otherwise, set $k = k + 1$ and go to Step 3.

Remark 6. As our system has only one varying parameter ω_e , it is also convenient to apply the *gridding-based* LPV synthesis [17], [26], [43]. The idea is to define a grid \mathcal{G} for $[\underline{\omega}_e, \bar{\omega}_e]$, then minimize γ under the LMIs defined by (11) with all $\omega_e \in \mathcal{G}$. Then check if the obtained P_1 and P_2 satisfy (11) under a denser grid. If it fails, increase the density of \mathcal{G} and resolve the LMIs. The girding-based method is easy to be implemented but such a method does not provide any rigorous guarantees for global convergence and performance [17].

C. Comparisons with different types of observer gains

In this subsection, we compare the designed parameter-varying observer gain with other approaches:

Constant Gains: In the observer gain design procedure outlined in the previous subsection, one possible choice is a Lyapunov function $V(e) = e^T Pe$, where P is independent of ω_e . This simplification leads to a more straightforward synthesis of the observer gain, as the quadratic terms in (11) become affine in ω_e , and $\frac{\partial P}{\partial \omega_e} = 0$. As a result, the polytopic LPV synthesis method from [35] can be applied, yielding only two LMI constraints for $\omega_e = \underline{\omega}_e$ and $\omega_e = \bar{\omega}_e$, as described

in (14a), with $P = P_1 = P_2$. The constant observer gain is then given by:

$$K = P^{-1}C^T R^{-1}.$$

Key points regarding this design are as follows:

- The design of a constant gain is more conservative than the one presented in Corollary 1, as the Lyapunov function $V(x)$ is independent of the parameter. Consequently, the solution to the LMIs in (14a) may not exist, since a common Lyapunov function for A_1 and A_2 may not exist in a quadratic form $e^T Pe$ with a constant P .
- The robust performance, denoted γ , may degrade with a constant gain, and at times, one might need to sacrifice robustness in order to ensure convergence.
- An observer with a constant gain lacks sensitivity to variations in speed, which can result in a sluggish response during rapid speed changes and may even lead to overshooting when dealing with a wide speed range.

In conclusion, to increase the possibility of obtaining a solution from (14a) with a constant P , adjustments to the system or observer may be necessary. These adjustments include assuming that the magnetic uncertainties are slow-varying (i.e., $d(t) = 0$) or even constant (i.e., $c(t) = 0$), as well as narrowing the speed range $[\underline{\omega}_e, \bar{\omega}_e]$.

Linear Time-Varying (LTV) Gains: Recall the results from [2], where a linear time-varying (LTV) observer was designed for torque estimation in PMSMs. In this design, the observer gain $K(t) = P^{-1}(t)C^T R^{-1}$ is calculated by solving the time-varying Riccati equation, similar to the original Kalman observer [30]:

$$\frac{dP(t)}{dt} = -A^T(t)P(t) - P(t)A(t) - P(t)QP(t) + C^T R^{-1}C, \quad (17)$$

where $A(t) = A(\omega_e(t))$ is treated as a time-varying matrix by incorporating the online estimate of ω_e . We now compare the LPV observer proposed in this paper with the LTV observer from [2]:

- The system model in [2] assumes that magnetic uncertainties satisfy $\dot{g}_d = \dot{g}_q = 0$, which limits its observer to handling only slow-varying uncertainties. In contrast, the proposed model Σ_e in (6) addresses magnetic uncertainties by treating \dot{g}_d and \dot{g}_q as state variables, with \ddot{g}_d and \ddot{g}_q treated as disturbances. This allows the observer to accommodate both slow and fast-varying uncertainties.
- A major challenge in LTV observer synthesis is ensuring the solvability of the time-varying Riccati equation (17). Even if $\Sigma(\omega_e(t))$ is observable at each time instant, this does not guarantee the solvability of (17), which requires uniform complete observability [30]. In contrast, the existence of an LPV observer gain $P(\omega_e)$ can be pre-verified through the solvability of the LMIs in (14a) and (14b).
- Another advantage of the LPV observer approach is its computational efficiency. The LPV observer gain is computed offline, whereas the LTV observer requires online computation of $P(t)$ by solving the time-varying Riccati equation (17), which can be computationally intensive.

V. SIMULATION RESULTS

A WRSM with the parameters shown in Table I is simulated in the MATLAB/Simulink environment. The model is based on the formulation presented in (6), where the dynamics of the magnetic uncertainties g_d , g_q and g_f are taken into account. A standard PI field-oriented controller is applied to the machine. Simulations are conducted to verify the effectiveness of the proposed method under significant tests involving magnetic uncertainties ΔM_f and ΔL_d . The first test involves a maximal 18% variation in M_f , while the second test examines a maximal 30% variation in L_d .

Parameters	Value
Maximum Power	65 KW
Number of pole pairs (p)	2
Stator winding resistance (R_s)	0.0123 Ω
Stator's d -axis inductance (L_d)	0.0017 H
Stator's q -axis inductance (L_q)	0.00065 H
Self inductance of field winding (L_f)	1.35 H
Mutual stator-rotor inductance (M_f)	0.0283 H
Moment of inertia	0.022 $Kg.m^2$
Coefficient of viscous friction	0.0064 Nm.s

TABLE I: WRSM Parameters of the first ZOE car.

These tests are conducted at low speeds (between 500 rpm and 600 rpm) of the WRSM under different torque commands. The rationale for selecting this specific speed range is discussed in Section VI-D. The torque is accurately estimated during both motor mode (when the torque command is increasing) and braking mode (when the torque command is decreasing). We compare three different torque estimation results with the reference/command torque, T_{Command} . The torque T_{LPV} is the estimation from the proposed LPV observer. The LPV gain is calculated as follows. The tuning matrices R and Q are chosen as

$$R = I_3, \quad Q = \text{diag}\{0.01, 0.1, 1, 0.01, 10, 6000, 1000, 10\}.$$

The values of the constant matrices P_1 and P_2 calculated through inequalities (14) are

$$P_1 = 10^3 \begin{bmatrix} 0.0051 & 0.0016 & 0.1154 & 0.7951 & -0.2419 & 0.0019 & 0.0130 & 0.0150 \\ 0.0016 & 0.0044 & 0.0370 & 1.3026 & -0.0336 & -0.0011 & 0.0215 & 0.0000 \\ 0.1154 & 0.0370 & 5.0404 & 19.3714 & -0.8417 & -0.0496 & 0.3158 & 0.7245 \\ 0.7951 & 1.3026 & 19.3714 & 682.5846 & -34.9667 & -1.6622 & 11.1293 & 0.0106 \\ -0.2419 & -0.0336 & -0.8417 & -34.9667 & 36.8094 & -0.4223 & 0.6589 & 0.0240 \\ 0.0019 & -0.0011 & -0.0496 & -0.1662 & -0.4223 & 0.0214 & -0.0260 & -0.0004 \\ 0.0130 & 0.0215 & 0.3158 & 11.1293 & -0.6589 & -0.0260 & 0.1875 & 0.0002 \\ 0.0150 & 0.0000 & 0.7245 & 0.0106 & 0.0240 & -0.0004 & 0.0002 & 0.1447 \end{bmatrix}$$

and

$$P_2 = 10^3 \begin{bmatrix} 0.0000 & 0.0000 & 0.0002 & 0.0032 & -0.0005 & -0.0000 & 0.0000 & 0.0000 \\ 0.0000 & 0.0000 & 0.0000 & 0.0013 & -0.0001 & -0.0000 & 0.0000 & 0.0000 \\ 0.0002 & 0.0000 & 0.0074 & 0.1010 & -0.0067 & -0.0002 & 0.0002 & 0.0007 \\ 0.0032 & 0.0013 & 0.1010 & 3.5314 & -0.2397 & -0.0709 & 0.0067 & 0.0002 \\ -0.0005 & -0.0001 & -0.0067 & -0.2397 & 0.1390 & 0.0000 & -0.0006 & 0.0000 \\ -0.0000 & -0.0000 & -0.0002 & -0.0079 & 0.0000 & 0.0000 & -0.0000 & -0.0000 \\ 0.0000 & 0.0000 & 0.0002 & 0.0067 & -0.0006 & -0.0000 & 0.0000 & 0.0000 \\ 0.0000 & 0.0000 & 0.0007 & 0.0002 & 0.0000 & -0.0000 & 0.0000 & 0.0001 \end{bmatrix}.$$

Thus the observer gain according to Corollary 1 is given by $K(\omega_e) = P^{-1}(\omega_e)C^T R^{-1}$, where $P(\omega_e) = \alpha(\omega_e)P_1 + (1 - \alpha(\omega_e))P_2$.

The torque T_{LTV} is the estimation from an LTV observer similar to that in [3], thus its gain is calculated online by solving (17). The torque T_{constant} comes from a constant gain (Luenberger-like) observer, where the gain is solved by equation (14a) with the assumptions that g_d , g_q and ω_e are constant to ensure a solution from (14a).

A. Results with magnetic uncertainties on mutual inductance

Figure 1 illustrates the torque estimation results over a span of 50 seconds. This analysis includes both static and dynamic variations in mutual inductance M_f . It is evident that the LPV observer performs excellently in tracking a piecewise constant torque reference, which is a common scenario in real-life driving conditions. Figure 2 presents a comparison of observers during the initial 10 seconds. Notably, during the dynamic changes occurring between 3 and 6 seconds, the robust LPV observer precisely estimates the electromagnetic torque, whereas the LTV method encounters difficulties in correcting torque estimation errors, particularly at $t = 2$ seconds. This issue is likely due to challenges in solving the time-varying Riccati equation, highlighting the reliability of the LPV approach. Additionally, from 2 to 3 seconds, the LPV observer consistently outperforms the LTV method. The LPV method also demonstrates less overshoot compared to the LTV method when dealing with sudden changes, such as the step function at 6 seconds, in M_f . Overall, both the LTV and LPV techniques deliver accurate estimates of electromagnetic torque throughout the testing period, whereas the observer with constant gains experiences significant estimation errors due to its maladaptation to speed variations

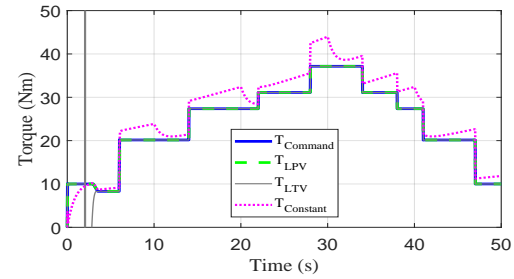


Fig. 1: Torque estimation results for 50s with uncertainties on M_f .

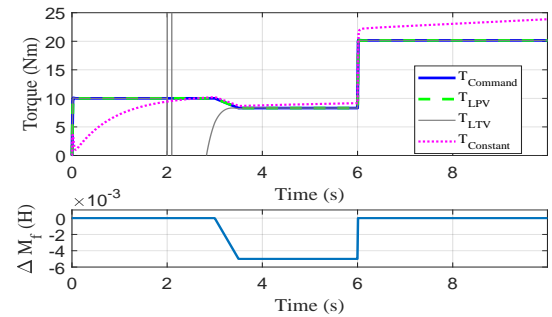


Fig. 2: Torque estimation results for 10s with uncertainties on M_f .

B. Results with magnetic uncertainties on stator inductance

Figs. 3 and 4 focus on variations in the stator's d -axis inductance L_d . This test is designed to highlight the effects of high-order derivatives of inductance variations. To simulate these effects, a sine function is used to modulate the d -axis inductance uncertainty. During the first phase of the simulation (from 0 to 4 seconds), the LTV observer displays significant

oscillations. This occurs because the LTV observer's design in [2] does not account for the presence of high-order derivatives of uncertainties, and the sine function introduces non-trivial high-order time derivatives that contradict this assumption. In contrast, the LPV method shows robustness against such high-order derivatives, providing a relatively accurate torque estimation during this period. Furthermore, the LPV method benefits from a simpler structure and lower computational costs for gain calculation, resulting in faster tracking performance. After the initial phase, both LTV and LPV methods deliver satisfactory torque estimations. In contrast, the constant gain observer exhibits a slow response and relatively large estimation errors throughout the entire simulation process..

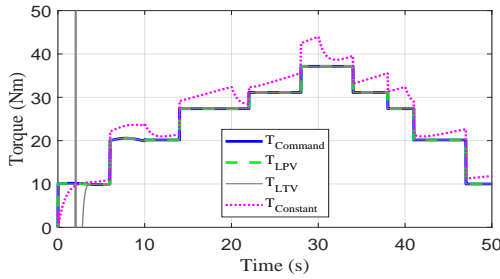


Fig. 3: Torque estimation results for 50s with uncertainties on L_d .

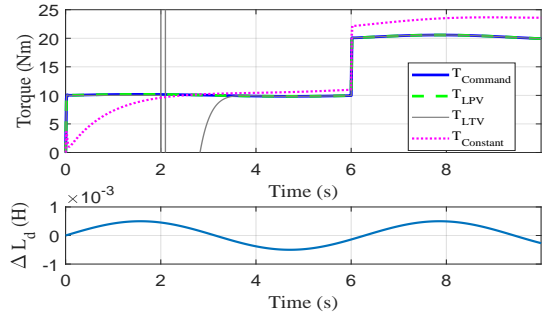


Fig. 4: Torque estimation results for 10s with uncertainties on L_d .

Remark 7 (Resistances uncertainties). The simulations with uncertainties in the resistances R_s and R_f have also been conducted. The estimation results show no significant differences when considering ΔR_s and ΔR_f to be zero or small values. The possible reasons for this have been explained in Remark 1 above. Specifically, the PI controller may compensate for the side effects caused by ΔR_s and ΔR_f , and the torque T_e of (2) has no direct connections with the resistances.

VI. EXPERIMENTAL RESULTS

A. Experiment setup

To assess the simulation results of the proposed observer based LPV approach, experiments tests are realized on the BE-MEVE test bench (<https://renault-chair.ec-nantes.fr/bemeve>), which is dedicated to test EV motors at 1-scale power level. The tested motor is a WRSM, which is used in the first generation of ZOE cars with the same parameters used in

simulation (Table I). As it can be seen in Fig. 5, the observers are developed in Matlab-Simulink environment. The control-Simulink file in which the observer is developed is compiled, and the generated code is loaded into the DSPACE real-time card. This generates the PWM signals that are sent to the inverter switches, which in turn generate the voltages V_a , V_b , V_c to be applied to the WRSM to impose the required command torque. Current sensors are integrated into the inverter and are the only measurements used by observers. The road profile is imposed by the DC Motor, whose speed is regulated by the associated speed controller via a chopper.

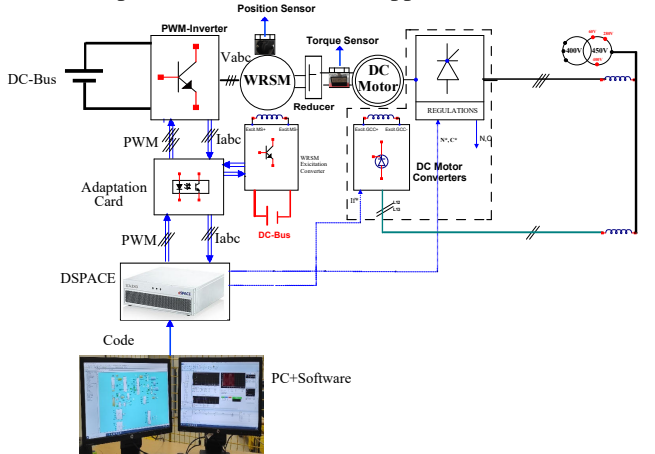


Fig. 5: Experimental setup details

B. Low speed (between 500 and 600 rpm) with different torque commands:

As in the simulation, this test corresponds to the driver's demand when pressing the car's acceleration pedal under a constant speed profile (road profile). The obtained results, shown in Figs. 6 and 7, are quite similar to those obtained in the simulation (Figs. 1 and 3). They reveal well-estimated torque when the torque command is increasing (motor mode) and decreasing (braking mode), despite the torque measurement being very noisy.

Remark 8. The simulation and experimental results are quite similar, though minor discrepancies remain. One possible reason is a mismatch between the current references and the voltage command required to generate the same torque. On the test bench, the current references are automatically generated from the torque command via a predefined table-matching algorithm. However, this is not the case in the simulations, where for a given desired torque T_e , the current references i_d and i_q are not uniquely determined, as indicated by (2). Another contributing factor is the absence of certain dynamic components in the simulation model, such as the PWM converter, which may influence the actual value of the commanded voltage.

We also notice the excellent performance of the torque estimation during dynamic phases of driving, such as rapid acceleration and deceleration. As expected, this performance is achieved by considering the higher-order time derivatives of the magnetic uncertainties g_d , g_q , which are managed by the proposed observer (9). The currents in the $d - q$ frame also

perform well. As shown in Fig. 7, they are estimated with high precision, contributing to the accurate torque estimation.

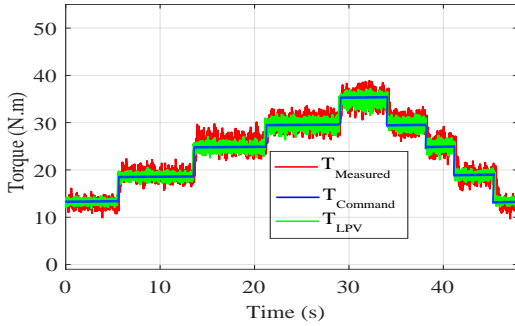


Fig. 6: Torque estimation results with the consideration of \hat{g}_d, \hat{g}_q .

In Table II, the experimental result of the estimated torque in Fig. 6 is compared to the simulation result in Fig. 1 in terms of MAE (Mean Absolute Error) and RMSE (Root Mean Square Error). It can be seen that the estimated torque (Fig. 1) obtained in simulation, has extremely low MAE and RMSE (0.001 N·m)). This is because the simulation conditions do not consider the dynamics of converters and reducer, the sensor inaccuracies, the measurement noise, the electromagnetic interference and the mechanical losses. However, in experimental conditions, the estimated torque (Fig. 6) shows significantly higher errors (MAE \approx 1.236 N·m, RMSE \approx 1.244 N·m). This is mainly due to the presence of real conditions that are neglected in simulation.

Metric	Simulation	Experimentation
MAE	0.001	1.236
RMSE	0.001	1.244

TABLE II: Comparison of Estimation Errors in Simulation and Experimentation

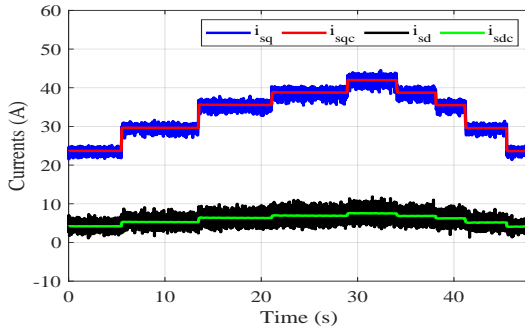


Fig. 7: The currents with the consideration of \hat{g}_d, \hat{g}_q .

C. Torque observer without uncertainties estimation:

To highlight the interest of the proposed observer, a test is conducted with constant speed and torque commands. In this test, the estimated values of uncertainties g_d and g_q are not included in the torque estimation (Fig. 8) during intervals of time $[0, 4s]$ and $[10, 14s]$. As can be seen, the torque estimation, during these intervals of time, does not perform well, a significant static error estimation appeared. Concerning the currents in the $d - q$ frame, they are well estimated (Fig. 9) since they do not depend on uncertainties estimation.

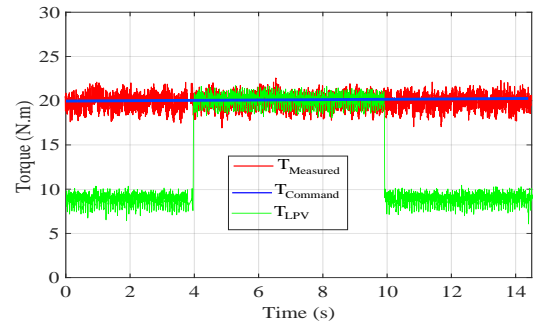


Fig. 8: Torque estimation without using \hat{g}_d, \hat{g}_q when $t \in [0, 4s]$ and $[10, 14s]$.

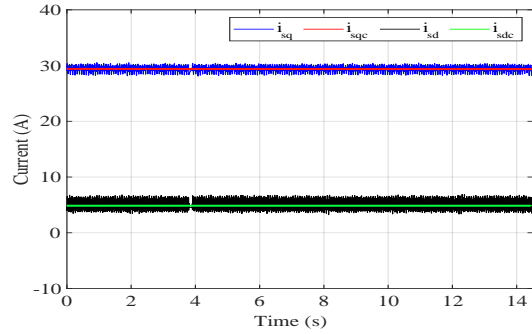
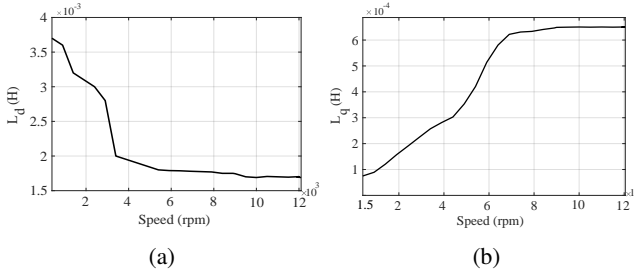


Fig. 9: The currents without considering \hat{g}_d, \hat{g}_q .

D. High speed validation:

In order to validate the proposed LPV-based torque observer at higher speeds, an additional experimental test was carried out close to the nominal speed range. As it can be observed in the low-speed region of Figs. 10a and 10b, the inductances identified in the $d - q$ axes (L_d and L_q) show significant deviations from their nominal values. These variations require the use of correction terms \hat{g}_d and \hat{g}_q within the observer to compensate for these deviations (see subsection VI-B). However, as rotor speed increases, the value of these inductances identified converge towards their nominal values, as shown in Figs. 10a and 10b. To further validate this behavior, an additional test was carried out close to the nominal speed range. In this test, the correction terms \hat{g}_d and \hat{g}_q are not used by the torque observer as it uses nominal inductance values. In fact, when the speed reaches the nominal regime, the correction terms \hat{g}_d and \hat{g}_q converge to zero, as illustrated in Fig. 12. The results, shown in Fig. 11, demonstrate that despite the absence of the correction terms \hat{g}_d and \hat{g}_q , the estimated torque (Fig. 11, green curve) closely aligns with the command torque (Fig. 11, blue curve). This indicates that at high speeds, the observer achieves an accurate torque estimate without the need to use \hat{g}_d and \hat{g}_q , as the inductances identified are sufficiently close to their nominal values. At nominal speeds, the system's behavior closely aligns with conventional estimation techniques based on constant nominal inductance values, reducing the computational load associated with real-time estimation of g_d and g_q .

It can be observed that in the low-speed operating mode, the inductances L_d and L_q exhibit significant deviations from their nominal values, behaving as uncertain or time-varying parameters. This is primarily due to the fact that low-speed

Fig. 10: Identified inductances L_d and L_q versus speed

operation typically demands high torque, which corresponds to high stator current. The resulting high current leads to magnetic core saturation, causing the inductance to vary nonlinearly with current. Consequently, magnetic parameter uncertainties in low-speed mode become non-negligible. In contrast, during high-speed operation, the inductances remain nearly constant, and their variations can often be neglected.

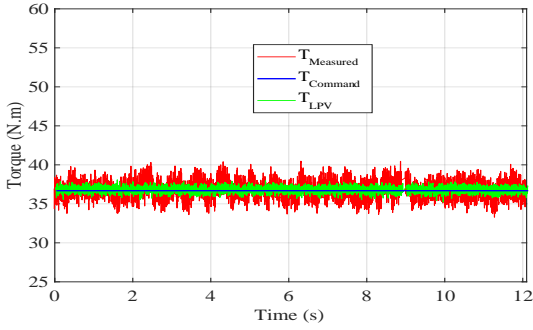
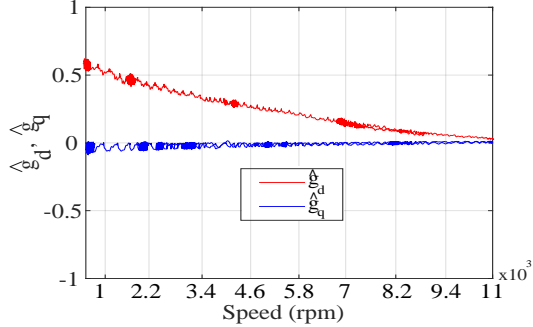


Fig. 11: Measured, command and estimated torque

Fig. 12: Correction gains \hat{g}_d and \hat{g}_q of LPV observer

E. Results comparison with different types of observers:

Experimental tests were conducted to support the comparison explanation given in Section IV-C and provide the readers with a direct understanding of the advantages of the proposed observer. The results obtained, with the same test conditions (low speed, parameters of Table I), are shown in Fig. 13. It can be seen that the proposed LPV observer performs well compared to the other two observers (LTV and constant gain observers) since the estimated torque of the proposed method (Fig. 13, green) follows closely the command torque (Figure 13, red). The constant gain observer estimates the torque with an important static error. This is because the gains are not adapted to the variation of the inductances and speed.

However, this observer is less consuming in terms of CPU since the gains are considered constants. For the LTV observer, a less static error (with respect to the case of constant gain) appears in the estimated torque (Fig. 13, black) compared to the torque command (Fig. 13, blue). This is because the observer considers the derivatives of the magnetic uncertainties constant. This LTV observer consumes much more in terms of CPU, since the matrix $P(t)$ used in its observer gain is computed online by solving a dynamic equation while it is computed offline in our proposed LPV observer. In addition, we tried to associate our modeling proposal with LTV observer, which should give a more close result to our proposed approach. However, we could not test it because it was overrun in real time due to the complex computation of the matrix $P(t)$ in real-time. A table of metrics for comparison of the performance of different observers is given in Table III.

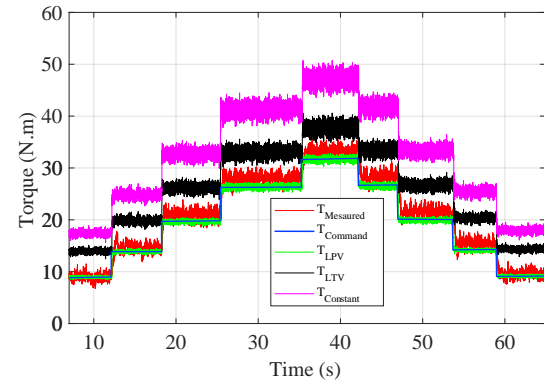


Fig. 13: Measured torque (red), LPV estimated torque (green), constant gains estimated torque (magenta), LTV estimated torque (black).

Criteria / Observer	Constant gain	LPV	LTV
Sampling time (μs)	100	100	100
Computation time (μs)	12.6	19.3	54.7
CPU load (%)	12.6	19.3	54.7
Mean square error (N.m)	5.50	0.008	2.82
Implementation complexity	Low	Medium	High
Risk of real-time overrun	Very Low	Low	High

TABLE III: Comparison of torque observers

VII. CONCLUSION

This article proposes a new technique for estimating the torque of wound rotor synchronous machines (WRSM) used in electric vehicles, particularly the Renault ZOE. This technique utilizes a sensorless approach to reduce costs and the congestion, while accounting for magnetic uncertainties and resistance variations. The innovation of this technique, compared to existing methods, lies in the design of a robust LPV state observer, ensuring precise torque estimation in both dynamic and static regimes despite the presence of uncertainties. An observability study of the WRSM and a rigorous proof of the observer's stability and robust performance are provided. The performance of the proposed LPV observer has been validated through simulation and experimental tests, and compared to two other observers of the type of constant gain and LTV. In contrast to the constant gain and LTV approaches, the LPV

observer offers a compromise between robustness to dynamic inductance variations and implementation cost, and ensures better accuracy. Hence, this technique demonstrates increased efficiency and robustness under real conditions, offering a solution to enhance the safety and control of electric vehicles. These results pave the way for future applications in various types of electric machines used in EVs.

ACKNOWLEDGMENT

This work is supported by the project Chair between Renault Group and Centrale Nantes about performances improvement of electric vehicles propulsion (<https://renault-chair.ec-nantes.fr/>).

REFERENCES

- [1] M. S. Rafaq, W. Midgley, and T. Steffen, "A review of the state of the art of torque ripple minimization techniques for permanent magnet synchronous motors," *IEEE Trans. on Ind. Inf.*, vol. 20, no. 1, pp. 1019–1031, 2023.
- [2] M. Taherzadeh, M. A. Hamida, M. Ghanes, and M. Koteich, "A new torque observation technique for a PMSM considering unknown magnetic conditions," *IEEE Trans. Ind. Electron.*, vol. 68, no. 3, pp. 1961–1971, 2020.
- [3] M. Taherzadeh, M. A. Hamida, M. Ghanes, and A. Maloum, "Torque estimation of permanent magnet synchronous machine using improved voltage model flux estimator," *IET Electr. Power Appl.*, vol. 15, no. 6, pp. 742–753, 2021.
- [4] M. Ghanes, M. Hamida, A. Maloum, and M. Taherzadeh, "Method for estimating the electromagnetic torque of a synchronous electric machine," February 9 2023, US Patent App. 17/760,084.
- [5] S. Patil, R. Saxena, and Y. Pahariya, "Simulation performance of brushless DC Motor drive using sensorless back EMF detection technique," in *International Conference on Futuristic Technologies (INCOFT)*. IEEE, 2022, pp. 1–4.
- [6] V. S. Virkar and S. S. Karvekar, "Luenberger observer based sensorless speed control of induction motor with fuzzy tuned PID controller," in *International Conference on Communication and Electronics Systems (ICCES)*. IEEE, 2019, pp. 503–508.
- [7] M. Ghanes, M. Hamida, A. Maloum, and M. Taherzadeh, "Method for estimating the electromagnetic torque of a wound-rotor synchronous machine," 2023, wO2023062161 (A1), EPO.
- [8] J. Yang, W.-H. Chen, S. Li, L. Guo, and Y. Yan, "Disturbance/uncertainty estimation and attenuation techniques in pmsm drives-a survey," *IEEE Trans. Ind. Electron.*, vol. 64, no. 4, pp. 3273–3285, 2016.
- [9] T. Sebastian, "Temperature effects on torque production and efficiency of PM motors using NdFeB magnets," *IEEE Trans. on Ind. Appl.*, vol. 31, no. 2, pp. 353–357, 1995.
- [10] K. J. Meessen, P. Thelin, J. Soulard, and E. Lomonova, "Inductance calculations of permanent-magnet synchronous machines including flux change and self-and cross-saturations," *IEEE Trans. on Magnetics*, vol. 44, no. 10, pp. 2324–2331, 2008.
- [11] W.-H. Chen, J. Yang, L. Guo, and S. Li, "Disturbance-observer-based control and related methods-an overview," *IEEE Transactions on Ind. Electr.*, vol. 63, no. 2, pp. 1083–1095, 2015.
- [12] W.-H. Chen, "Disturbance observer based control for nonlinear systems," *IEEE/ASME Trans. on Mechatronics*, vol. 9, no. 4, pp. 706–710, 2004.
- [13] K.-S. Kim, K.-H. Rew, and S. Kim, "Disturbance observer for estimating higher order disturbances in time series expansion," *IEEE Trans. Autom. Control*, vol. 55, no. 8, pp. 1905–1911, 2010.
- [14] J. Han, "From PID to active disturbance rejection control," *IEEE Trans. Ind. Electron.*, vol. 56, no. 3, pp. 900–906, 2009.
- [15] H. K. Khalil, "Extended high-gain observers as disturbance estimators," *SICE Journal of Control, Meas., and Syst. Integr.*, vol. 10, no. 3, pp. 125–134, 2017.
- [16] X. Xu, H. Luo, M. Huo, Y. Jiang, X. Zhang, and X. Lv, "A robust integrated estimation of unknown disturbances, parameters and states for linear time-varying systems," *IEEE Trans. on Ind. Electr.*, 2025.
- [17] C. Hoffmann and H. Werner, "A survey of linear parameter-varying control applications validated by experiments or high-fidelity simulations," *IEEE Trans. Control Systems Technology*, vol. 23, no. 2, pp. 416–433, 2014.
- [18] A. Hanif, A. I. Bhatti, and Q. Ahmed, "Managing thermally derated torque of an electrified powertrain through LPV control," *IEEE/ASME Trans. on Mechatronics*, vol. 23, no. 1, pp. 364–376, 2017.
- [19] S. N. Ali, M. J. Hossain, D. Wang, K. Lu, P. O. Rasmussen, V. Sharma, and M. Kashif, "Robust sensorless control against thermally degraded speed performance in an IM drive based electric vehicle," *IEEE Trans. on Energy Conversion*, vol. 35, no. 2, pp. 896–907, 2020.
- [20] H. Zhang, G. Zhang, and J. Wang, " H_∞ observer design for LPV systems with uncertain measurements on scheduling variables: Application to an electric ground vehicle," *IEEE/ASME Trans. on Mechatronics*, vol. 21, no. 3, pp. 1659–1670, 2016.
- [21] H. Zhang, R. Wang, and J. Wang, *Robust Gain-Scheduled Estimation and Control of Electrified Vehicles via LPV Technique*. Springer, 2023.
- [22] Y. Lee, S.-H. Lee, and C. C. Chung, "LPV H_∞ control with disturbance estimation for permanent magnet synchronous motors," *IEEE Trans. Ind. Electron.*, vol. 65, no. 1, pp. 488–497, 2017.
- [23] A. Casavola and G. Gagliardi, "Fault detection and isolation of electrical induction motors via LPV fault observers: A case study," *Int. J. Robust & Nonlinear Control*, vol. 25, no. 5, pp. 627–648, 2015.
- [24] S. Ibrir, "LPV approach to continuous and discrete nonlinear observer design," in *IEEE Conf. Decis. Control*. IEEE, 2009, pp. 8206–8211.
- [25] Y. Wang, D. M. Bevly, and R. Rajamani, "Interval observer design for LPV systems with parametric uncertainty," *Automatica*, vol. 60, pp. 79–85, 2015.
- [26] M.-H. Do, D. Koenig, and D. Theilliol, "Robust H_∞ proportional-integral observer-based controller for uncertain LPV system," *J. Franklin Inst.*, vol. 357, no. 4, pp. 2099–2130, 2020.
- [27] I. Khalil, J. Doyle, and K. Glover, *Robust and Optimal Control*. Prentice hall, 1996, vol. 2.
- [28] S. Boyd, L. El Ghaoui, E. Feron, and V. Balakrishnan, *Linear Matrix Inequalities in System and Control Theory*. SIAM, 1994.
- [29] L. Li, G. Pei, J. Liu, P. Du, L. Pei, and C. Zhong, "2-DOF robust h_∞ control for permanent magnet synchronous motor with disturbance observer," *IEEE Transactions on Power Electr.*, vol. 36, no. 3, pp. 3462–3472, 2020.
- [30] R. Kalman and R. Bucy, "New results in linear filtering and prediction theory," *Journal of Basic Engineering*, vol. 83, no. 1, pp. 95–108, 1961.
- [31] P. Gahinet, P. Apkarian, and M. Chilali, "Affine parameter-dependent Lyapunov functions and real parametric uncertainty," *IEEE Trans. Autom. Control*, vol. 41, no. 3, pp. 436–442, 1996.
- [32] O. Wallmark, L. Harnefors, and O. Carlson, "An improved speed and position estimator for salient permanent-magnet synchronous motors," *IEEE Trans. Ind. Electron.*, vol. 52, no. 1, pp. 255–262, 2005.
- [33] A. Messali, M. Ghanes, M. A. Hamida, and M. Koteich, "A resilient adaptive sliding mode observer for sensorless AC salient pole machine drives based on an improved HF injection method," *Control Engineering Practice*, vol. 93, p. 104163, 2019.
- [34] A. Messali, M. A. Hamida, M. Ghanes, and M. Koteich, "Estimation procedure based on less filtering and robust tracking for a self-sensing control of IPMSM," *IEEE Trans. Ind. Electron.*, vol. 68, no. 4, pp. 2865–2875, 2020.
- [35] P. Apkarian, P. Gahinet, and G. Becker, "Self-scheduled H_∞ control of linear parameter-varying systems: A design example," *Automatica*, vol. 31, no. 9, pp. 1251–1261, 1995.
- [36] R. Hermann and A. Krener, "Nonlinear controllability and observability," *IEEE Trans. Autom. Control*, vol. 22, no. 5, pp. 728–740, 1977.
- [37] G. Conte, C. H. Moog, and A. M. Perdon, *Algebraic Methods for Nonlinear Control Systems*. Springer Science & Business Media, 2007.
- [38] R. Hirschorn, "Invertibility of multivariable nonlinear control systems," *IEEE Trans. Autom. Control*, vol. 24, no. 6, pp. 855–865, 1979.
- [39] W. Respondek, "Right and left invertibility of nonlinear control systems," in *Nonlinear Controllability and Optimal Control*. Routledge, 2017, pp. 133–176.
- [40] A. Isidori, *Nonlinear Control Systems*, 3rd ed., ser. Communications and Control Engineering Series. Berlin: Springer-Verlag, 1995.
- [41] Q. T. Dinh, S. Gumussoy, W. Michiels, and M. Diehl, "Combining convex-concave decompositions and linearization approaches for solving BMIs, with application to static output feedback," *IEEE Trans. Autom. Control*, vol. 57, no. 6, pp. 1377–1390, 2011.
- [42] Y. Wang, R. Rajamani, and A. Zemouche, "A quadratic matrix inequality based PID controller design for LPV systems," *Syst. Control Lett.*, vol. 126, pp. 67–76, 2019.
- [43] P. Apkarian and R. Adams, "Advanced gain-scheduling techniques for uncertain systems," *IEEE Trans. Control Systems Technology*, vol. 6, no. 1, pp. 21–32, 1998.